INFRA SWEDEN 2030

Project Report on

Automatic detection of railway fasteners and track defects

2018-03-26

(Diarienummer 2016-03306)

Praneeth Chandran, Hakan Lind, Johan Odelius, Ulf Ranggård, Matti Rantatalo

INFRA SWEDEN 2030

Contents

INFRA SWEDEN 2030

LIST OF FIGURES

1 Acknowledgement

The project team would like to acknowledge Vinnova and InfraSweden 2030 for their financial support (Diarienummer 2016-03306). The project team would also like to acknowledge Thomas Nordmark and Lars Sundholm representing Trafikverket for facilitating numerous field measurement occasions along the iron ore line.

2 Introduction

In view of mobilization and transportation of people and commodity rail transportation plays a significant role. In addition, it forms a major contributing factor in economic and industrial development of a nation. The railway infrastructure has a huge investment. With approximately €15-25 billion spent on railway asset maintenance, maintenance managers are striving to cut maintenance costs through effective predictive maintenance. Often railway tracks are responsible for nearly half of all delays to passenger and safety issues mainly due to railway track maintenance and renewal of network [1]. The researchers are evolving application of RAMS(Reliability, Availability, Maintainability and Safety) to asset management of railway track to integrate them with LCC (Life cycle costing), maintenance planning, to optimize the cost and reduce interventions. Inspection on regular basis of the track for physical defects and design non-compliances, becomes highly necessary, to maintain safe and efficient operations. Such track inspections are required to cover a wide spectrum, ranging from detecting surface cracks in the rail, measuring rail profile and rail spacing (gauge), to monitoring the conditions of joints, spikes and anchors [2]. The environment in which rail works are, harsh and they are constantly subjected to complex and variable forces. The rail surface are subjected to constant cyclic load and are thus prone to metal fatigue which can result in partial or complete failure. The rail is a structural unit within the track construction that demands immediate rectification even on the slightest failure. One of the other crucial component in rail track is the rail fastening system, which acts as a means of fixing rails to sleepers. Fig 1. Shows a rail fastening system with its various components.

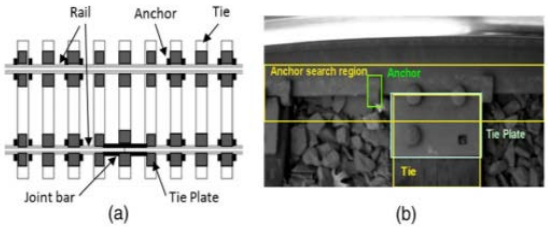

Figure 1 Illustration of (a) rail fastening system and (b) targeted rail components [2]

Traditionally trained inspectors, who walk along the track length and search for rail damages, carry out the task of track inspection. The risk associated with this method is substantially high. It is highly error prone, expensive and time consuming, for railroad companies specifically for long-term and large-scale development. With the extension of high-speed railway network, the inspection and maintenance face more challenges than ever before [3]. In recent time, measuring, track's curvature and alignment, cross-level of the two rails, have been already automated by employing a track geometry car. However, railroad track inspectors still manually

and visually conduct other inspections, such as monitoring the rail surface, spiking and anchor patterns and detecting raised or missing spikes and anchors. In order to lower maintenance costs, enhance safety and increase track capacity, railroad companies are laying more emphasis on substituting the current manual inspection process using machine vision technology for more efficient, effective and objective inspections.

This report gives a brief description about fastening systems and surface defects in rail track in section 2 and 3 respectively. Further, it reviews some of the work from early 2000's for fastener inspection, measurement and detection in section 4. In addition, it discusses the advantages and limitations of these methods and thereby pointing out the necessity to concentrate on an alternative approach to overcome these limitations. Section 5 gives a description on the proposed measurement system. The experimental approach explaining the test track at Luleå Tekniska Univesitet, field test, and the apparatus setup are described in section 6. The results from the field and lab tests are analysed in depth in the same section. Section 7 gives a brief conclusion based on the results obtained from this project.

3 Rail Fastening System

Rail fasteners are components that are used to fix rails on to sleepers, preventing the rails from unexpected separation when the train passes through. The fastening system usually comprises rail anchors, rail tie plates, chairs, fasteners, spikes, screws bolts etc. Figure.2 shows a fastening system and its components

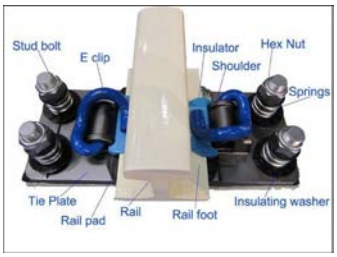

Figure 2 Components of rail fastening system

Rail anchors are spring steel clips used to prevent longitudinal movement of the rail, due to either vibrations or fluctuations in temperature. They are attached to the underside of the rail baseplate and bear against the sides of the sleepers. The tie or base plate is used to hold the rail to correct gauge and to increase the bearing area. These are steel plates that are fastened to wooden ties by means of spikes or bolts through the holes in the plate.

Common types of fastenings (Figure 3) are- fastening with rail spike with base plate above the tie, E-clip Fastening, Pandrol Fast Clip Fastening and Heyback fastening, the name of which may vary with locations

Figure 3 - types of rail fastenings (LTU Test Track)

3.1 Inspection classes

In Sweden, the inspection intervals for railway assets are based on different track classes- B1, B2. B3, B4 and B5. Each class is defined based on the individual traffic load and speed associated with it. The classes are defined based on the following conditions (refer Figure.3).

- Class B1
  - Speed: less than or equal to 40 km/h
- Class B2
  - Speed: higher than 40 km/h but less or equal to 80 km/h

- Traffic load: less than or equal to 8 MGT/track/year
- Class B3 (Option 1)
  - Speed: higher than 40 km/h but less or equal to 80 km/h
  - Traffic load: higher than 8 MGT/track/year
- Class B3 (Option 2)
  - Speed: higher than 80 km/h but less or equal to 140 km/h
  - Traffic load: less than or equal to 8 MGT/track/year
- Class B4 (Option 1)
  - Speed: higher than 80 km/h but less or equal to 140 km/h
  - Traffic load: higher than 8 MGT/track/year
- Class B4 (Option 2)
  - Speed: higher than 140km/h
  - Traffic load: less than or equal to 8 MGT/track/year
- Class B5
  - Speed: higher than 140km/h
  - Traffic load: higher than 8 MGT/track/year

Figure 4 Inspection classes with respect to million gross tonnage and speed [REF TDOC]

When a track section is assigned, a specific inspection class, some aspects other than speed and trainload has to be considered like-

- Traffic type e.g. dangerous goods.
- Climate and environmental conditions.
- Geotechnical properties
- Technical structure and design
- The inherent reliability of the asset
- Age and quality of the asset.

Additionally, business and socioeconomic aspects can also affect the decision when an inspection class is assigned to a track.

3.2 Railway fasteners inspection

For fasteners, the inspection intervals are dependent on the inspection class B1-B5. The fasteners are grouped in to the track group, which have the following inspection intervals, see Table 1

Table 1 Inspection intervals for track and hence fasteners for different inspection classes

Class	B1	B2	B3	B4	B5
Inspections per year	1	2	3	3	3

For each inspection event, the following points should be checked-

- The track gauge should not be risked to go out of defined maintenance limit, for joint free or welded tracks
- The clamp spring of the fastener should have enough clamp force to clamp the insulator and the rail
- Not more than four clamping springs or four shoulders should be missing or damaged within a distance of 20 sleepers. Of these, a maximum of two may be missing or injured in consequence.
- that no scratches from clamping springs are found on the rail foot or insulator (signs of altered rail amount or rail change due to low clamping force)
- that the insulator is not missing or damaged and has not slid out of position

For fasteners in switches and crossings (S&C) the following points must be checked-

- That no remarks can be found on the fasteners, especially close to the switchblade tip.
- That all fasteners are intact and that nothing is missing where the switch blade is operating
- That the isolators are intact and in position
- That not more than 3 under plates per 10 sleepers are missing or more than 2 screws from these under plates

4 Rail Surface Defects

The speed and load of the trains have been increasing rapidly over the past few years to match and aid the economical and industrial development of the society. The rail is constantly subjected to various stresses including, bending and shear stresses, contact stresses, thermal stresses and residual stresses. These factors inevitably raise the risk, of the rail being subjected to defect formation. The riding quality and safety of the railway system can be tarnished by these surface defects. Rail surface defects can be classified in to two broad categories based on the manner and periodicity they occur- Discrete or non-periodic and periodic defects. Discrete defects are individual or groups of non-periodic defects that appear on the rail head in random or arbitrary manner without any characteristic repetition or periodicity. These defects can be induced by traffic or from other surface anomalies (e.g. error in manufacturing process). Some of the common discrete defects are discussed in general below [26]

- ***Engine or Wheel burn*** :- defects that occur as a pair on both sides of the rail head, opposite to each other as a result of slipping or sliding of the locomotive
- ***Railhead damage***: - local damages to the surface of rail caused by wheel flats, broken wheels or dragging equipment.
- ***Weld irregularities***: - it is the non-uniformity of the rail surface at welds, manifesting as a result of improper finishing or batter accumulation.
- ***Battered Joints***: - these are the degradation of the ends of the rail, located near joint bars, formed as a result of multiple impact of wheels on the end of the rail.
- ***Mismatched Joints***: - Joints in the rail that are not matched properly. They lead to discontinuity in the running surfaces of the rail resulting in high wheel-impact forces.
- ***Shelly Spots***: - are degradation found at the gage corner of the high rail. They are also referred to as Spalling. It manifests itself initially as micro cracks (headchecks), and propagates further to larger areas.
- ***Squats***: - are rolling contact fatigue defects found near the centre of the railhead. They are similar to headchecks but they grow down internally.

Shelling, gage-corner shelling, crushed head, plastic flow, surface roughness and mill defects are some other types of non-periodic defects found on the rail surface. Periodic defects are those that appear on the rail surface in a periodic or repeatable manner. The most common periodic defect is corrugation, which are waves of discontinuities on the surface of railhead. Rail defects can also be narrowed down to three broad categories based on the source of origin, as follows –

- Originating from rail Manufacturing defects- battered defects, kidney defect or tache oval etc.
- Originating as a result of inappropriate handling, installations and use – wheel burn defects etc.
- Originating due to the exhaustion of rail steels resistance to fatigue damage – most kinds of RCF (squats, headchecks, etc.)

Recent developments in steel and rail manufacturing technology has helped to address and minimize most of the rail defects caused by manufacturing faults. A strong intervention and

superior supervision from railways and railway service industries can minimize the rail defects due to inappropriate handling, installations and usage. Rail Defect Management (RDM) traditionally targets to minimize the defects and failures in these two categories. Increase in freight load and speed has led to increase in the defects on the surface of the rail over the past few decades. Failures involving RCF have become one of the serious concern for railway maintenance management. One of the best example pointing towards the consequence of RCF is the derailment at Hatfield in UK, October 2000, resulting from head checking. These surface initiated RCF pose special inspection concerns and hence there is a need to incorporate an efficient and sophisticated inspection method to detect these at an early stage.

5 Prior Works

5.1 State of art for fastener inspection

Machine vision have been gradually adopted by the railway industry as a track inspection technology, since the pioneering work by *Cunningham et al*. [4, 5]. These first generation visual inspection systems were capable of collecting and storing images of rail, for a later review. However, these systems failed to facilitate automated detection in the early 2000's due to lack of fast processing hardware. In 2007 *Marino et al*. [6, 7, 8], introduced their VISyR system which was a fully automatic and configurable FPGA-based vision system for real-time infrastructure inspection, able to analyse defects of the rails and to detect the presence/absence of the fastening bolts that fix the rails to the sleepers. The system was able to acquire images of the rail by means of a DALSA PIRANHA 2 line scan camera [Matrox] having 1024 pixels of resolution and using the Cameralink protocol. It uses two 3-layer neural networks running in parallel to detect hexagonal-headed bolt. To indicate the fastener, a binary output is generated, by taking 2-level discrete wavelet transform (DWT) of a 24x100 pixel-sliding window (their images use non-square pixels) for the two networks, as an input. The first NN uses Daubechies wavelets, while the second one uses Haar wavelets and these wavelet decomposition is equivalent to performing edge detection at different scales with two different filters. Same set of samples were used to train both the networks and the final decision were made based on the maximum output of each network. The VISyR system is designed for mostly detecting the presence/absence of fasteners; however, they do not give significant information about defects or cracks on the same. Moreover, the result may be inaccurate when the shape and environment of the fastener is complex (example-VOSSLOH fastener).

In 2008 *Babenko* [9], used an image based detecting device comprising of two industrial laser range scanners (one for each rail), to detect missing or defective fasteners. A convolutional filter bank was applied directly on these intensity images. Each type of fastener had a single filter associated with it, whose coefficients were calculated using an illumination-normalized version of the Optimal Trade-off Maximum Average Correlation Height (OT-MACH) filter [10]. These detectors however, were not tested for longer track section and do not indicate the impact of the environmental parameters. *Resendiz et al*. [11] adopted a track cart to capture video of railroad track with off-the-shelf cameras and recorded these data to an on-board laptop. To determine the location of rail component such as crossties and turnouts a texture classification with a bank of Gabor filter followed by an SVM was adopted. MUSIC algorithm was encompassed to locate spectral signature to define expected component locations. The algorithm however does not give any indications to possible defects of the fasteners or its robustness to external parameters.

Visual inspection of fasteners have predominantly dominated over the past two decades, but the detection methods have varied over time. *Marino et al*. [8] used a multilayer perceptron neural classifier to detect missing hexagonal-headed bolts. *Stella et al* [12] used a neural classifier for locating the missing fasteners (Hook-shaped), employing wavelet transform and principal component analysis. *J.Yaang et al* [13] adopted direction field as the template of fastener and matched using linear discriminant analysis to obtain the weight coefficient matrix. *Ruvo et al* [14], adopted error backpropagation algorithm, to model mainly two type of fasteners. To achieve real time performance the detection algorithm was implemented on

graphical processing unit. For automatic detection of hexagonal bolts, *Ruvo et al* [15] also adopted a FPGA based architecture using the same algorithm. The above-mentioned techniques were successful in detecting fasteners but failed to give significant information on defective ones. Xia et al [16] used AdaBoost training for hook-shaped fastener, departing the fastener in to four part and training each with AdaBoost, thus enabling it to detect worn out fastener. *Li et al* [17] and *Rubinsztejn* [18] used the same algorithm to detect fasteners and its components. These works were concentrated on specific fastener type and do not provide information about the robustness on illumination variation, which is one of the key feature in image processing. Gabor filters [19], Edge detection methods [20], Support Vector Machine (SVM) [21], are some of the other widely used techniques for modelling and detecting fasteners. The above-mentioned discriminative models can classify the fastener and non-fastener samples but find it difficult to indicate partially worn out or defective fasteners. Common generative models used for fastener detection include Latent Dirichlet allocation (LDA) [22] and structure topic model (STM) which is an extension of LDA. *H.Feng et al* [23] used STM to model fasteners, as it was able to learn the probabilistic representations of different objects using unlabelled samples.

5.2 State of art for rail surface defects inspection

Over the past century, rail failures has remained to be a significant problem and the existing maintenance procedure model developed based on rail damage present in the rail network are neither sufficiently accurate nor efficient enough to eliminate the need for inspection [27]. Non-destructive evaluation (NDE) methods are considered as a strong tool for rail surface inspection and have been used for the same since early 1877 [28]. The first mode of high-speed inspection involved using a magnetic induction sensor, [29, 30] in Sperry test vehicle (named after Dr. Sperry who developed the inspection vehicle), which was followed by ultrasonic transducers in 1953 [30].

Rail inspection using ultrasonic transducers have gained significant importance as it can be used for both manual and high-speed inspection. The inspection speed achieved through this method varies from 15-80 Km/h [31, 32]. It was able successfully to detect surface defects, railhead internal defects, rail web and foot defects [33]. However, the present conventional ultrasonic probes fails to detect small headchecks and gauge corner cracking during high-speed inspection. The presence of small surface cracks may sometime submerge the more critical internal defects while analysing. Rail inspection using magnetic induction (Magnetic Flux Leakage-MFL) [34, 35, 36] are carried out, usually for speed up to 35 Km/h. MFL have proved to be a strong tool for detecting surface defects and near surface internal railhead defects. MFL cannot however detect cracks that are smaller than 4mm and their signal strength deteriorates at a speed higher than 35Km/h. Rail inspection using pulsed eddy current (PEC) sensor was able to overcome the challenges faced by the ultrasonic transducers, and it was able to detect RCF, wheel burns, grinding marks and short wave corrugation [37, 38, 39, 40]. PEC sensors can be used to a maximum speed of 70 Km/h, but are severely affected by lift off variations and are prone to classify grinding marks as small cracks. Automated Visual inspection can be used up to a speed of 320 Km/h and are a strong tool in detecting defective ballast, surface breaking defects and rail head profile, however they require huge investment and surface treatment. They also cannot asses the rail for internal defects [41]. Radiography are used for manual inspection for static tests on weld and known defects [42, 43]. However, they are not efficient in detecting certain

transverse crack and have many health and safety drawbacks. Long-range ultrasonic, Laser ultrasonic, alternating current field measurement sensors (ACFMs), electromagnetic acoustic transducers (EMATs), Acoustic Emission and Acoustic emission Pulsing are some of the recent NDE technology that are under development stage for rail surface detection. A detailed state of the art for rail surface detection will be presented in the near future.

Automated visual inspection is an expensive technique to carry out, especially for long-term projects and long distance measurements. The optimum condition for detection of different fasteners and its complicated geometry make this technique less effective. Most of the current models are suited to inspect the presence of a particular fastener but they do not give sufficient information about the condition of the same. Automated visual inspection becomes a challenge when, the fastener and the rail is obscured due to dust coverage, surface erosion, rusting, brightness fluctuation and motion blurring. The major drawback of this method is its lack of ability to detect the rail surface and the fasteners, submerged under snow, covered by stones and other debris or under heavy rain. This calls in for additional surface treatment or removal process that adds to the expense of the railroad companies.

Therefore, an effective and sophisticated alternative approach for fastener inspection needs to be explored. NDT (Non-Destructive Testing) plays an important role in CBM of railways. One of the popular method of NDT in railway is using UT (Ultrasonic Testing). The need for surface treatment before testing and the difficulty to study the display of the test result make it a complex method. The ultrasonic testing of the weld of inside the railhead is advantages in accuracy and intuition, but it is incapable to detect the defect on the surface or near the surface of the rail [24]. Eddy current based inspection can overcome the major challenges mentioned above. In addition, the inspection technique we propose have the advantage of incorporating both the rail surface and the fasteners, thus minimizing the overall cost of the inspection. The presence of non-conductive materials in the sensor-to-target gap do not affect eddy current sensors. This allows their use in dirty environments-dirt, water, oil, snow and machine fluids-where other displacement sensor technologies fail. Another advantage of this technique is that there is minimal or no, need for surface treatment.

The current research aims on railway track signatures and anomaly detection in modulated magnetic fields from an eddy current based sensor.

6 Measurement System

Since decades, eddy current method is well known for the non-destructive testing of electrically conductive objects [44, 45]. Eddy current testing are also applied to examine surface cracks on the rail [46]. Eddy currents are local circular currents, which are created or generated when a varying magnetic field meets a conducting material. The eddy currents themselves create a secondary magnetic field, which tends to cancel out the driving field at the local point of the surface. In principle, the proposed eddy current sensor (Lindometer) is sensitive to local fluctuations of the conductivity (σ), magnetic permeability (μ) and geometric form of the material. Hence, such sensors can be used to detect inhomogeneities along the rail track, e.g. rail clamps and irregularities of the rail [47].

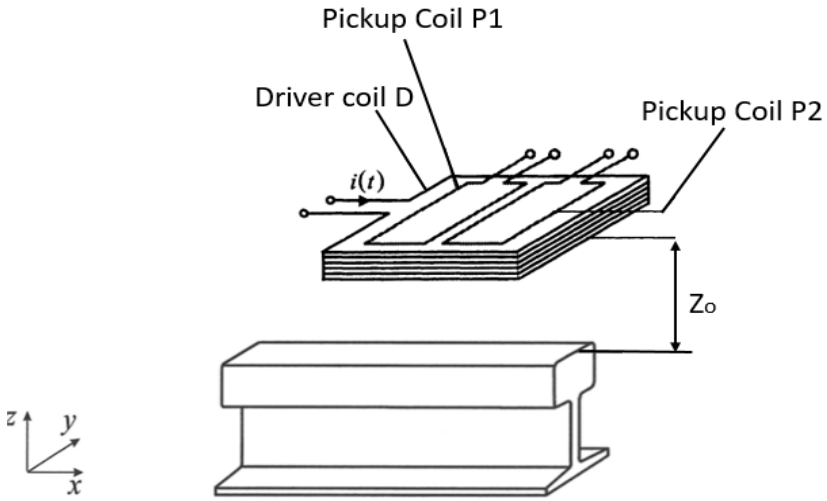

Figure 5 Arrangement of the Lindometer sensor coil

For the application to train based measurements, differential eddy current sensors are preferred. Figure 1 shows the proposed sensor, consisting of a driver coil 'D' and two pickup coils 'P1' and 'P2'. The driving coil is driven by a sinusoidal pr imary current i(t), which generates an alternating primary magnetic field. Eddy currents are thus induced within the rail located in the proximity of the sensor. A secondary magnetic field is generated as a result of these eddy current, which has an opposite direction to the primary field, confiding with Lenz's law.

The Lindometer uses a driving field with frequencies of 18 kHz and 27 kHz to detect variations in amplitude, phase and a combination of both. The above-mentioned frequencies are taken as the carrier frequencies as these frequencies fall under the rail norms. The information along the rail is represented as the variations in amplitude or phase or a combination of both which are extracted and analysed by demodulation techniques. The size of the driving coil is approximately 18(z), 70(x), and 155(y) mm. The driving coil acts as an outer winding enclosing the pick-up coils. The winding is applied in one layer with N=22 turns with a copper diameter of 0.7mm. The pick-up coils have a dimension 18(z), 30(x) and 150(y) mm, and each coil has a winding applied in one layer with 94 turns and a copper diameter of 0.16mm. The two coils are placed side by side in x-direction with a gap of 4mm in the centre of the coil system.

The two pick-up coils are enclosed by the driving coil and differentially coupled as shown in figure 2. The two frequencies have a common factor of 9 kHz, which gives the opportunity to cancel out the small cross talk between them by the inbuilt Cross Talk Cancellation (CTC) function. The direct cross talk between the driver and pick-up coil is cancelled out but not completely, by the differentially coupled pick-up coils. The resulting voltage u(t) is the result of the cross-talk residue and the induction of eddy currents along the rail which are linearly superimposed. The quality of the cross-talk cancellation is a question of geometrical symmetry between the three coils and hence the windings are placed in an even layer with no crossovers. The entire unit is vacuum potted with epoxy resin to stabilize the sensor, both against vibrations and to reduce temporary drift.

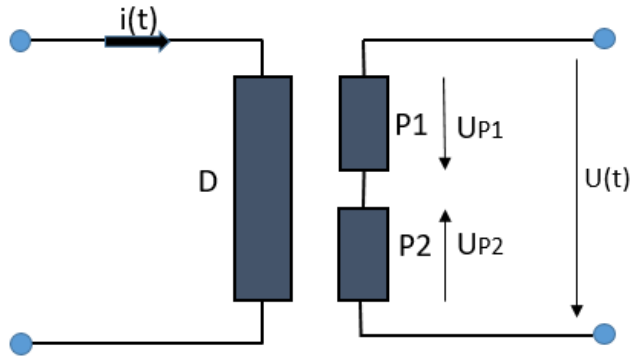

Figure 6 Circuit Diagram of the sensor system

The driving coil generates eddy current in the rail and vicinity in the 'x-y' plane. The pick-up coils are sensitive only to the z-component of the generated flux from the eddy current due to the geometrical orientation as shown in figure.1. The differentially coupled pick-up coils (P1-P2) are sensitive only to changes in the eddy current in the rail and its vicinity and not any absolute value can be detected. If there is an even surface with no change in conductivity (σ), magnetic permeability (μ) or geometric form of the material, as an ideal rail with no clamps or any surface defects, the resulting voltage u(t) will be zero due to induction of similar eddy currents all over the place. Assume a change in μ or σ or geometry at one single point at the railhead, while other parts are the very same and therefore create similar eddy currents. Due to the symmetry of the differentially coupled pick-up coils, only the singular point with 'the eddy current change' will create a signal given by the equation below.

$$u(t) = P1v(t) – P2\ v(t)$$

The resulting signal u(t) will be a function of the relative distance between the single point eddy current source and two pick-up coils. The angle 'Θ' must also be considered in x-direction as the driving flux density varies significantly along the x-axis. Due to the symmetry of the differentially coupled pick-up coils, there is zero induction u(t) when the source is just below the symmetry line of the pick-up coil (Figure 3.a), positive induction to the left (Figure 3.b), and negative induction to the right (Figure 3.c)

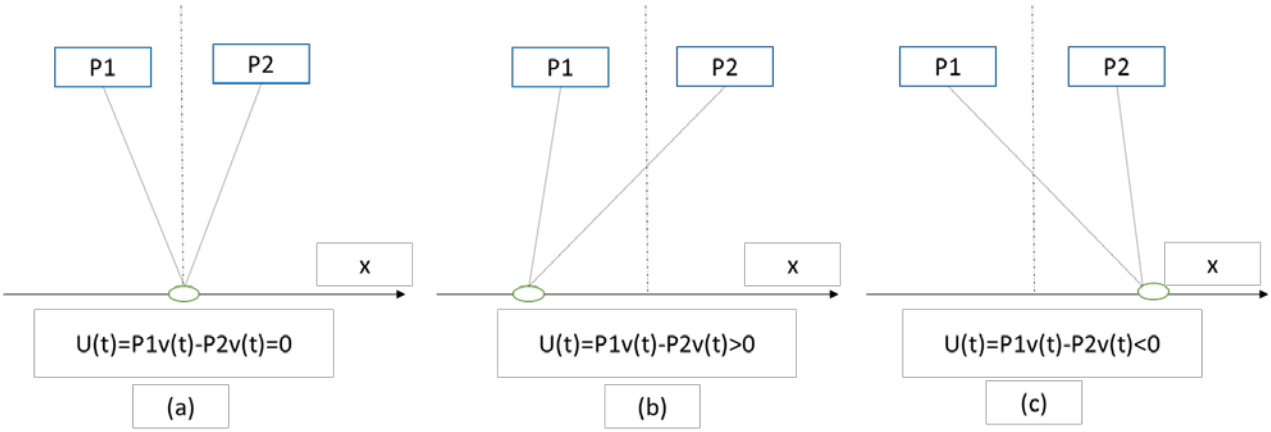

Figure 7induction in the differentially coupled pick-up coils due to the position of current source (a) source at the symmetry line (b) source to the left of the symmetry line (c) source to the right of the symmetry line

7 Measurements

7.1 LTU test track

Figure 8 LTU test track

Measurements were carried out along the test track developed at Lulea University of Technology to investigate the response of the sensor to, different types of fastening systems (Refer Figure.3), presence of snow on the track. Measurements were also carried out to investigate sensor response to insulation joints along the track length.

7.2 Field Test May-June, 2017

Measurements were performed along the iron ore line at Katterjåkk and Stordalen, before and after grinding of the rail. These iron ore lines are located close to the Norway–Sweden border (close to Riksgränsen, one kilometre into Sweden). Figure 5 shows the iron ore line

Figure 9 Iron ore line at Katterjåkk and Stordalen

A complete damage free section of the track was not visible as there were some grinding marks or minute cracks along the full length. The track was inspected for various damages including cracks, grinding marks, squats, missing fasteners, etc. Figure 6 shows some of the damages observed in the track

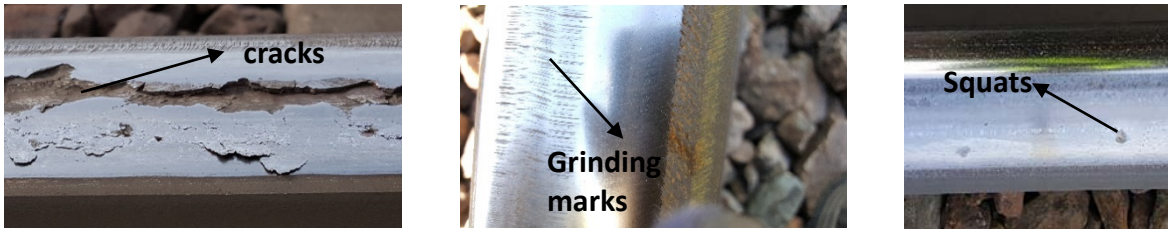

Figure 10 - Common damages found on the measurement track

E-Clip fastening (Refer figure 3) was the only type of fastening system visible along the entire track length.

7.2.1 Measurement Procedure

The Lindometer sensor was mounted on a trolley system as shown in figure 7 and was pushed along the track for carrying out the measurement (speed was not set to be uniform). The sensor was powered using a 12V62AH battery and the measurements were recorded using a laptop. The trolley was given three initial jerks to study the pattern of vibration on the sensor, in the recorded measurement.

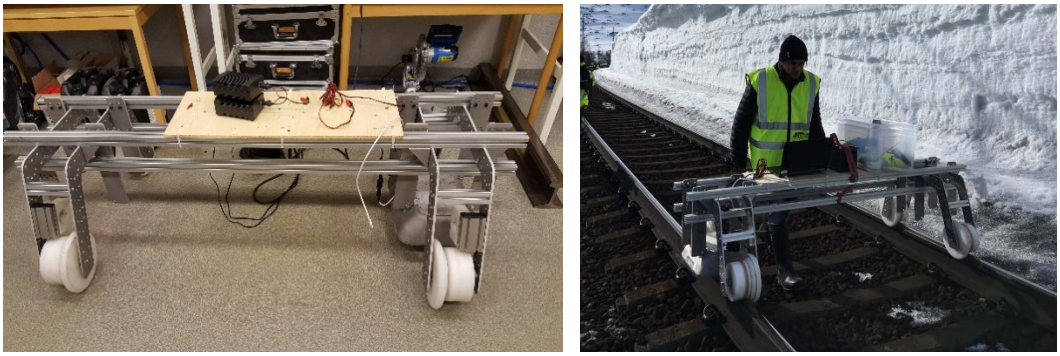

Figure 11 Lindometer Measurement setup

All the measurements were categorized with respect to various track conditions, as follows

- No rail defects and e-clip before grinding
- No rail defects and e-clip after grinding
- Rail defects and eclip before grinding
- Rail defects and eclip after grinding
- No rail defects and Heyback with insulation joint
- No rail defects and Rail Spike or Pin Clip with insulation joint

7.2.2 Results

7.2.2.1 No rail defects and e-clip before grinding

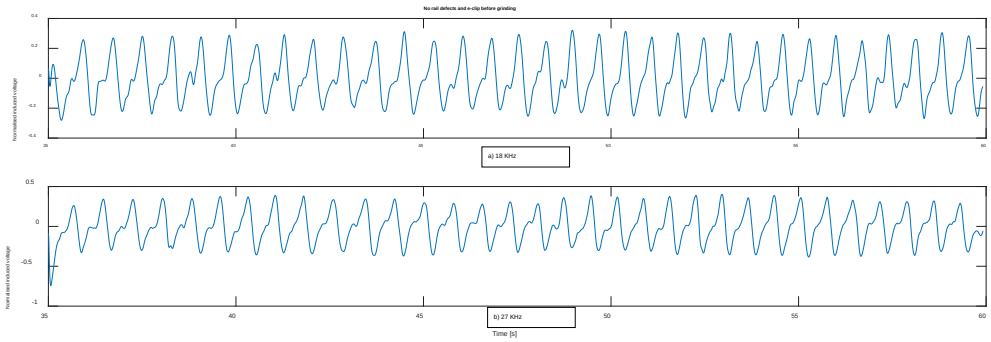

Figure 12 before grinding, Time signal: (a) 18 kHz Demodulation angle 83.3 degrees and (b) 27 kHz Demodulation angle 223.24 degrees, Measurement of a track section with minimal amount of defects on the track. All fasteners are in place.

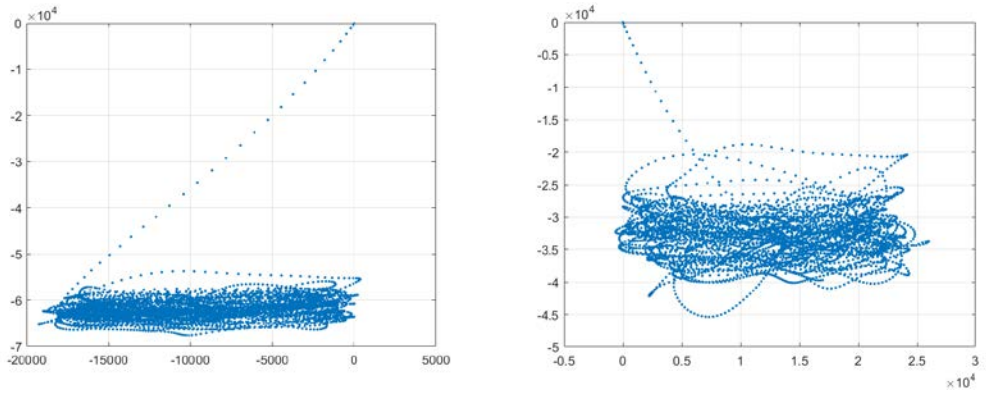

Figure 13 Before grinding, I/Q plot of the demodulated signals: (a) 18 kHz Demodulation angle 83.3 degrees and (b)27 kHz Demodulation angle 223.24 degrees, Measurement of a track section with minimal amount of defects on the track. All fasteners are in place.

Figure 12 shows the time signal of the measurement carried out for a relatively healthy portion of the track before grinding. Individual clamps can be easily distinguished from both 18 KHz and 27 KHz plots. The IQ plot of the demodulated signal (Figure 13) is evenly distributed in a straight pattern without significant deviations. The demodulation angle was fixed at 83.3 degrees for 18 KHz and 223.24 degrees for 27 KHz.

7.2.2.2 No rail defects and e-clip after grinding

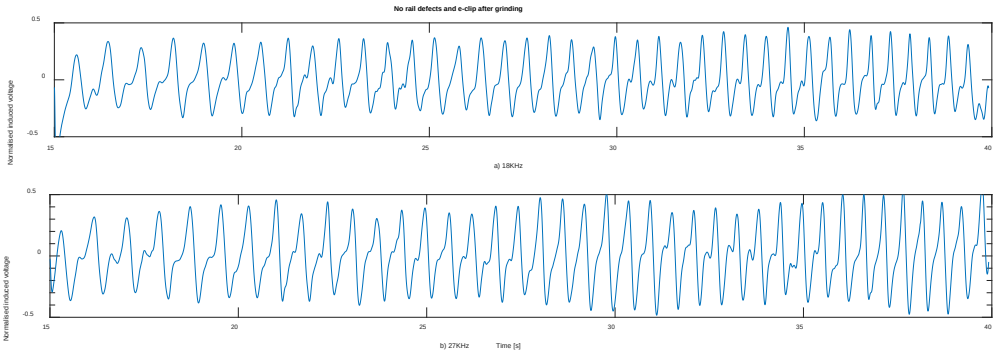

Figure 14 after grinding, Time signal: (a) 18 kHz Demodulation angle 83.3 degrees and (b) 27 kHz Demodulation angle 223.24 degrees, Measurement of a track section with minimal amount of defects on the track. All fasteners are in place.

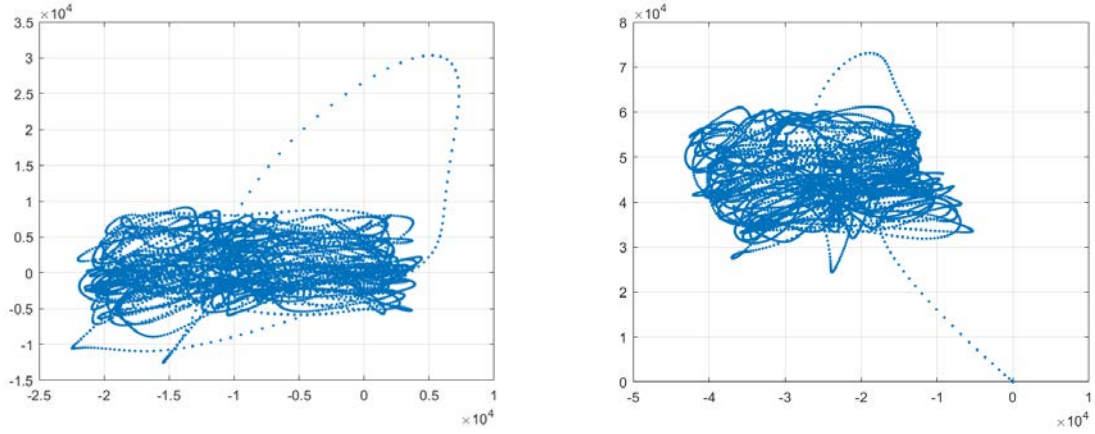

Figure 15 After grinding, I/Q plot of the demodulated signals: (a) 18 kHz Demodulation angle 83.3 degrees and (b) 27 kHz Demodulation angle 223.24 degrees, Measurement of a track section with minimal amount of defects on the track. All fasteners are in place.

Figure 14 shows the time signal of the measurement carried out for a relatively healthy portion of the track after grinding. Individual clamps can be easily distinguished from both 18 KHz and 27 KHz plots. Amount of grinding carried out in this track was minimal as it was without much cracks. There is a slight increase in the magnitude of the time signal but the difference was not significant. The IQ plot of the demodulated signal (Figure 15) is evenly distributed in a straight pattern without significant deviations. However, the distribution was not as smooth as compared to the one before grinding. The demodulation angle was fixed at 83.3 degrees for 18 KHz and 223.24 degrees for 27 KHz.

7.2.2.3 Rail defects and e-clip before grinding

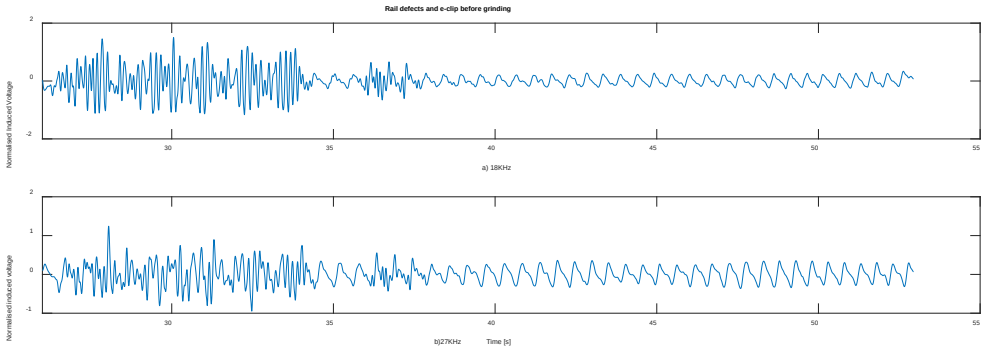

Figure 16 before grinding, Time signal: (a) 18 kHz Demodulation angle 83.3 degrees and (b) 27 kHz Demodulation angle 223.24 degrees, Measurement of a track section with defects on the track. All fasteners are in place.

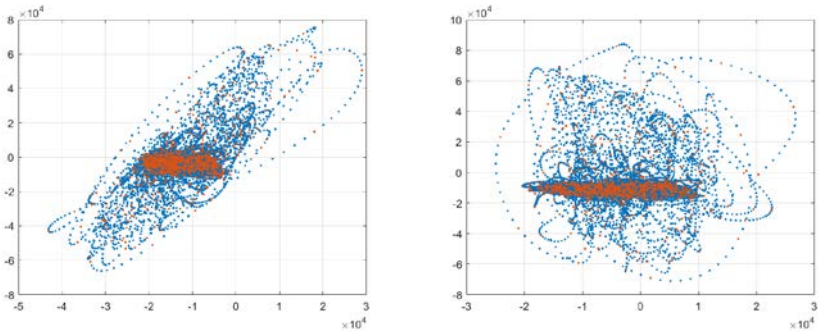

Figure 17 Before grinding, I/Q plot of the demodulated signals: (a) 18 kHz Demodulation angle 83 degrees and (b) 27 kHz Demodulation angle 210 degrees, Measurement of a track section with defects on the track. All fasteners are in place.

Figure 16 shows the time signal of the measurement carried out for a cracked portion of the track before grinding. The cracks were found at the initial parts of the track (within first 30 sleepers). Individual clamps can be easily distinguished from both 18 KHz and 27 KHz plots, in the crack free parts. The cracks are visible in the time signal with higher magnitude. The demodulation angle was fixed at 83.3 degrees for 18 KHz and 223.24 degrees for 27 KHz to observe the clamp features. The IQ plot of the demodulated signal (Figure 17) shows that the healthy clamp features follow a pattern similar to Figure 11, but the cracks are superimposed to these clamp signals, modulated at a different angle.

7.2.2.4 Rail defects and e-clip after grinding

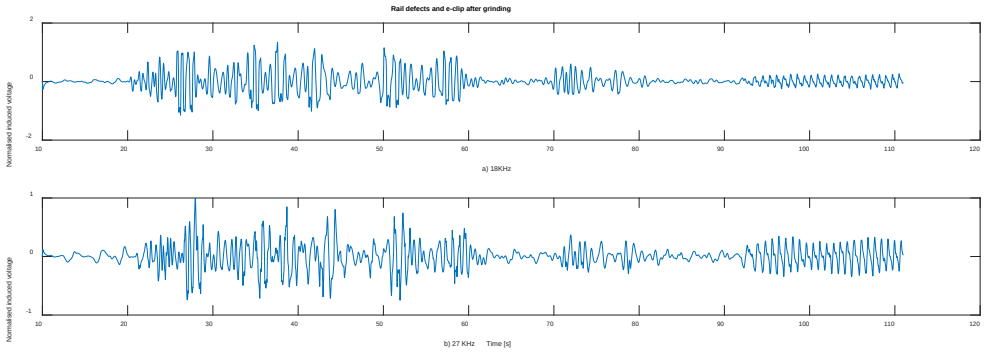

Figure 18 After grinding, Time signal: (a) 18 kHz Demodulation angle 83.3 degrees and (b) 27 kHz Demodulation angle 223.24 degrees, Measurement of a track section with defects on the track. All fasteners are in place.

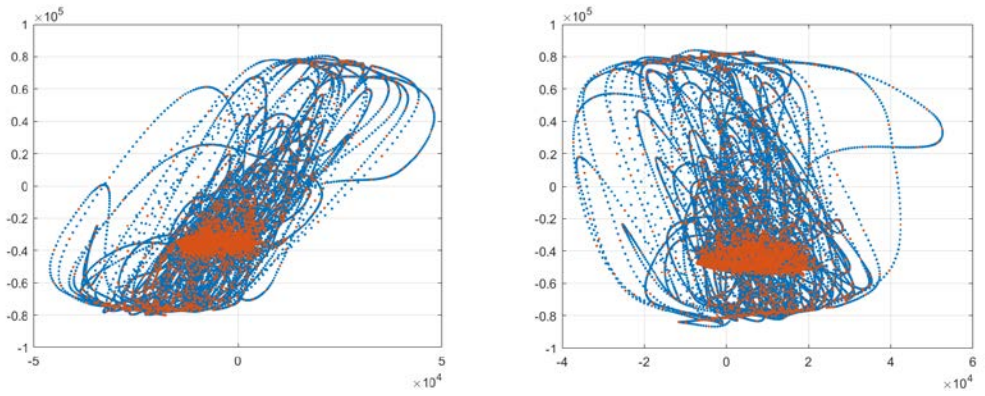

Figure 19 After grinding, I/Q plot of the demodulated signals: (a) 18 kHz Demodulation angle 83.3 degrees and (b) 27 kHz Demodulation angle 223.24 degrees, Measurement of a track section with defects on the track. All fasteners are in place.

Figure 18 shows the time signal of the measurement carried out for a cracked portion of the track after grinding. The cracks were found at the initial parts of the track (within first 30 sleepers). Individual clamps can be easily distinguished from both 18 KHz and 27 KHz plots in the crack free parts. The cracks are visible in the time signal with high magnitude, but slightly lesser compared to the ones before grinding. The demodulation angle was fixed at 83.3 degrees for 18 KHz and 223.24 degrees for 27 KHz to observe the clamp features. The IQ plot of the demodulated signal (Figure 19) shows that the healthy clamp features follow a pattern similar to Figure 11, but the cracks are superimposed to these clamp signals, modulated at a different angle. The IQ-plot distribution is also affected by the grinding marks present, as the difference is clearly visible when compared with the IQ-plot before grinding.

7.2.2.5 Identifying Vibration in Measurement with IQ-plot

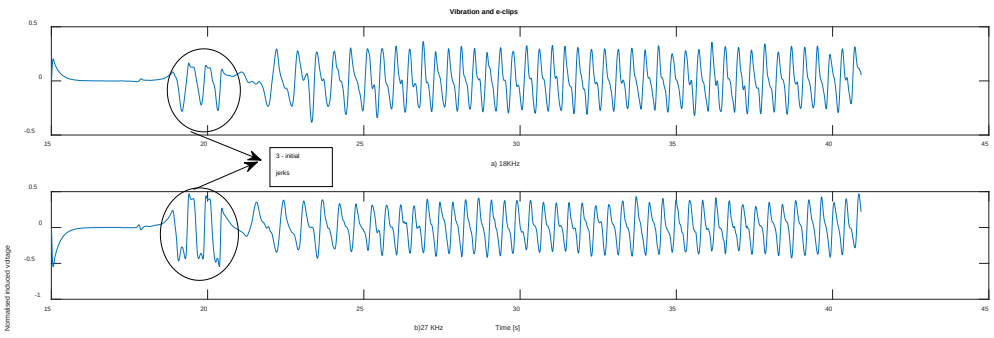

Figure 20 Time signal: (a) 18 kHz Demodulation angle 83.3 degrees and (b) 27 kHz Demodulation angle 223.24 degrees, Measurement of a track section with initial vibration on the sensor. All fasteners are in place.)

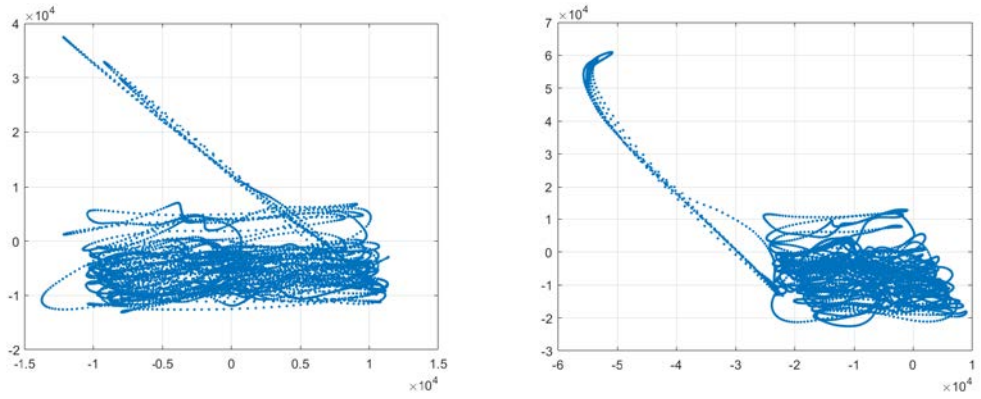

Figure 21 I/Q plot of the demodulated signals: (a) 18 kHz Demodulation angle 83.3 degrees and (b) 27 kHz Demodulation angle 223.24 degrees, Measurement of a track section with initial vibration. All fasteners are in place.

Figure 20 shows the time signal of the measurement carried out for a relatively healthy track section without any cracks. The three corresponding jerks are visible in the initial stages of the time signal (marked in the plot). The IQ plot (Figure 21) of the same measurement shows a deviation from the normal pattern distribution for a healthy track. The deviation corresponds to the vibration data and these are modulated at a different angle compared to the clamps and cracks.

7.2.2.6 Squats, Vibration and clamps

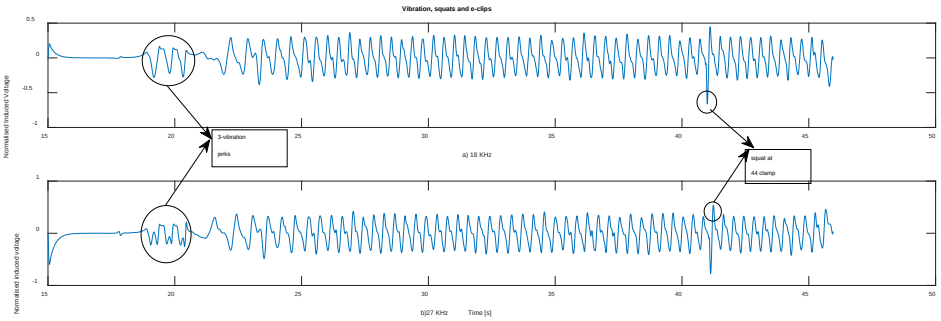

Figure 22 Time signal: (a) 18 kHz Demodulation angle 83.3 degrees and (b) 27 kHz Demodulation angle 223.24 degrees, Measurement of a track section to identify the vibration on the sensor. All fasteners are in place.

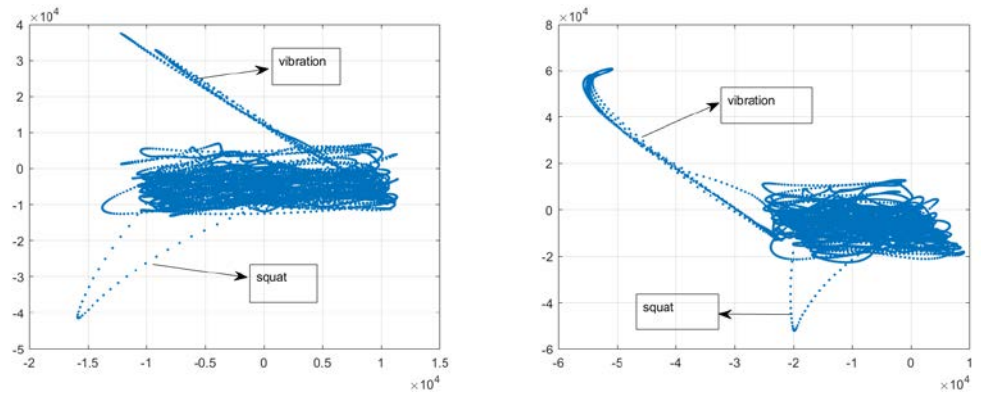

Figure 23 I/Q plot of the demodulated signals: (a) 18 kHz Demodulation angle 83.3 degrees and (b) 27 kHz Demodulation angle 223.24 degrees, Measurement of a track section with initial vibration. All fasteners are in place.)

Figure 22 shows the time signal of the measurement carried out for a relatively healthy track section with a squat located at the 44th sleeper. The three corresponding jerks are visible in the initial stages of the time signal (marked in the plot). The presence of the squat is visible as there is a hike in the magnitude. The IQ plot (Figure 23) of the same measurement shows two deviations from the normal pattern distribution for a healthy track. The first deviation corresponds to the vibration data and is similar to the case explained in figure 17.b. The second deviation corresponds to the squat present in the track.

7.2.2.7 Missing Clamp

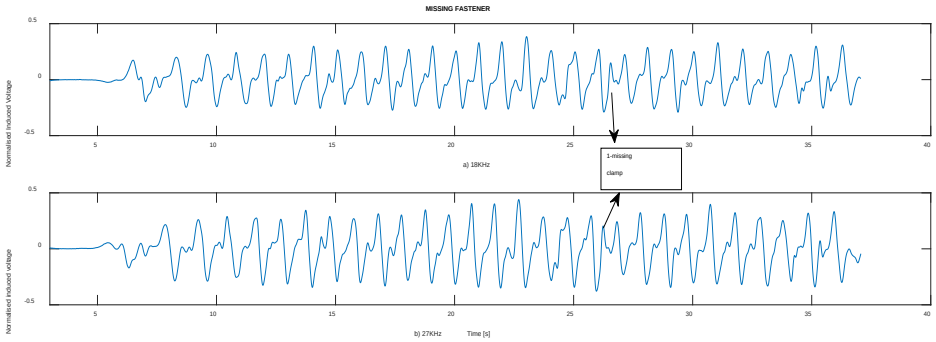

Figure 24 Time signal: (a) 18 kHz Demodulation angle 83.3 degrees and (b) 27 kHz Demodulation angle 223.24 degrees, Measurement of a track section to identify the pattern of missing clamp. (1-missing clamp)

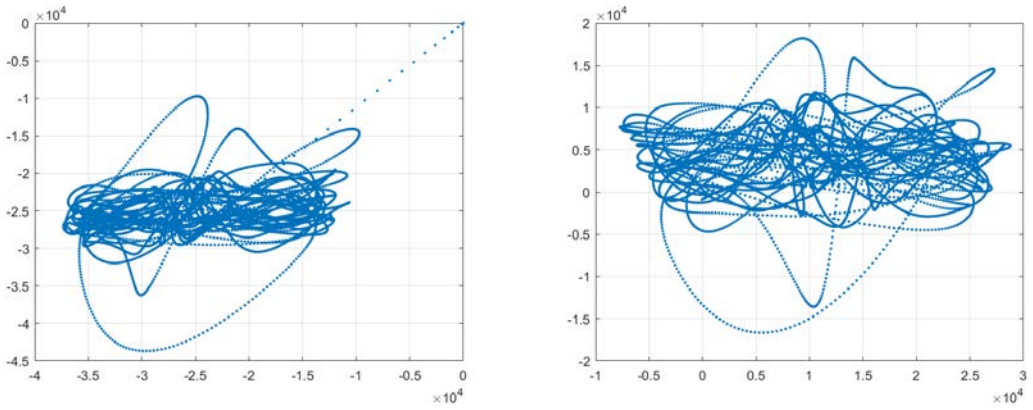

Figure 25 I/Q plot of the demodulated signals: (a) 18 kHz Demodulation angle 83.3 degrees and (b) 27 kHz Demodulation angle 223.24 degrees, Measurement of a track section to identify the pattern of missing clamp. (One missing clamp)

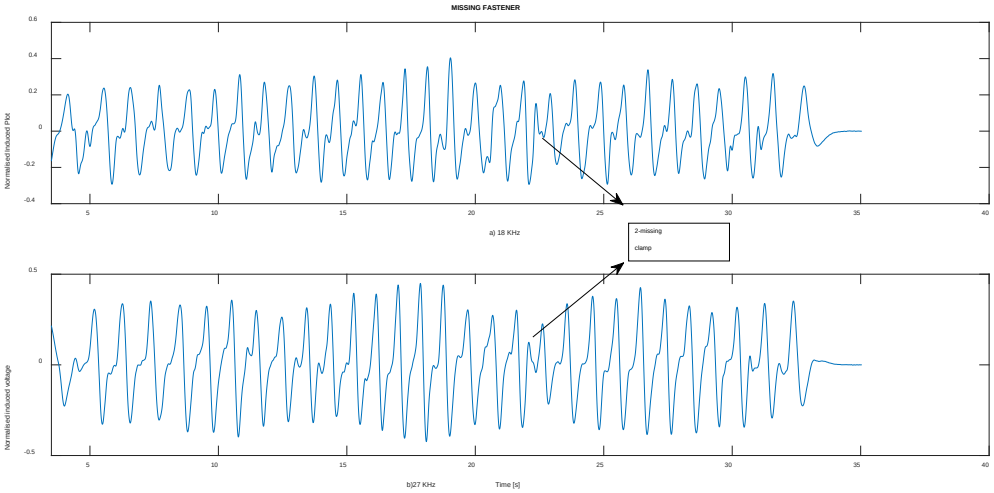

Figure 26 Time signal: (a) 18 kHz Demodulation angle 83.3 degrees and (b) 27 kHz Demodulation angle 223.24 degrees, Measurement of a track section to identify the pattern of missing clamp. (2-missing clamp)

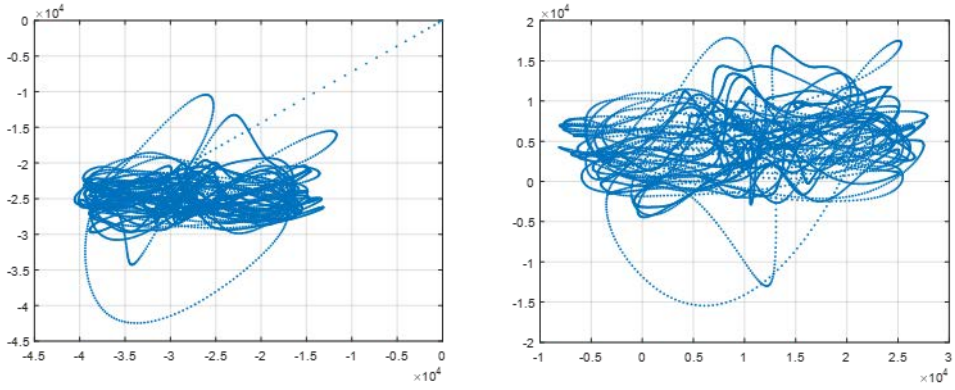

Figure 27 I/Q plot of the demodulated signals: (a) 18 kHz Demodulation angle 83.3 degrees and (b) 27 kHz Demodulation angle 223.24 degrees, Measurement of a track section to identify the pattern of missing clamp.(2-missing clamp)

Figure 23 and Figure 25 shows the time signal for measurements carried out to detect missing fasteners. Clamps (one and two respectively) was removed from the track at the same sleeper position and the plot shows a corresponding change in pattern as marked in the figure. The IQ-plot (Figure 24 and Figure 26) also shows a change from normal behaviour.

7.2.2.8 No defects and Heyback fastening with Insulation Joint

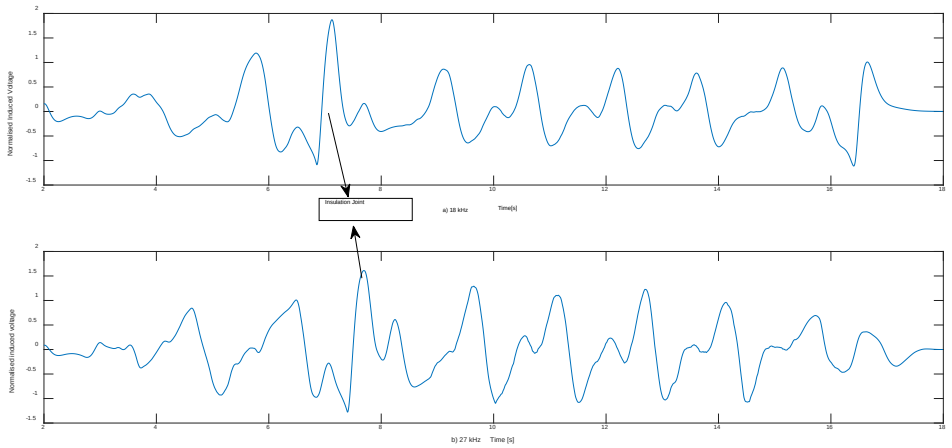

Figure 28 Time signal (a) 18 kHz Demodulation angle 182 degrees and (b) 27 kHz Demodulation angle 330 degrees, Measurements of lab test track to identify Heyback clip and Insulation joint

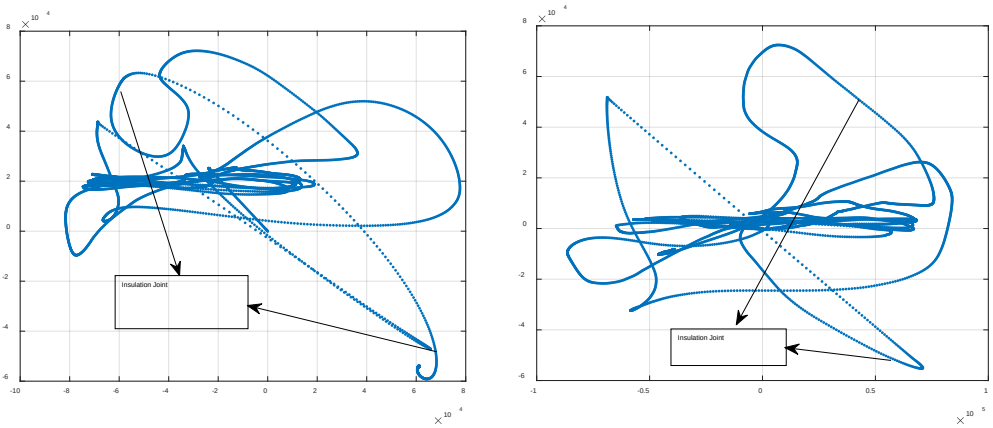

Figure 29 I/Q plot of the demodulated signals: (a) 18 kHz Demodulation angle of 182 degrees and (b) 27 kHz Demodulation angle 330 degrees. Measurement of a section of lab test track to identify Heyback clip and Insulation Joint.

Fi ealthy pc asily distinguished from both 18 KHz and 27 KHz plots. The demodulation angle was altered from that used for the E-clip fasteners. The IQ plot of the demodulated signal (Figure 29) shows that clamp features and insulation joints are modulated differently and can be distinguished from each other. The demodulation angle was fixed at 182 degrees for 18 KHz and 330 degrees for 27 KHz.

7.2.2.9 No Defects and Rail Spike with Insulation Joint

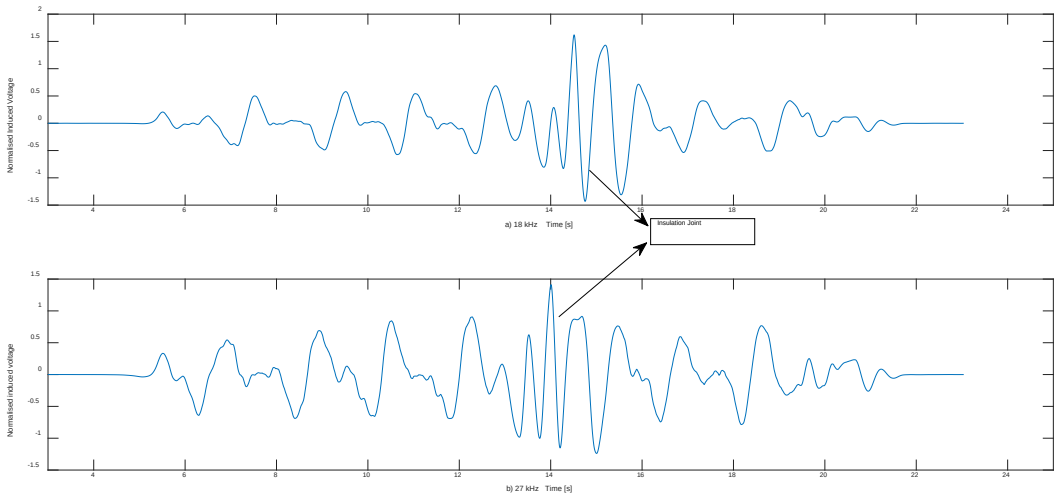

Figure 30 Time signal (a) 18 kHz Demodulation angle 177 degrees and (b) 27 kHz Demodulation angle 327 degrees, Measurements of lab test track to identify Rail Spike and Insulation joint

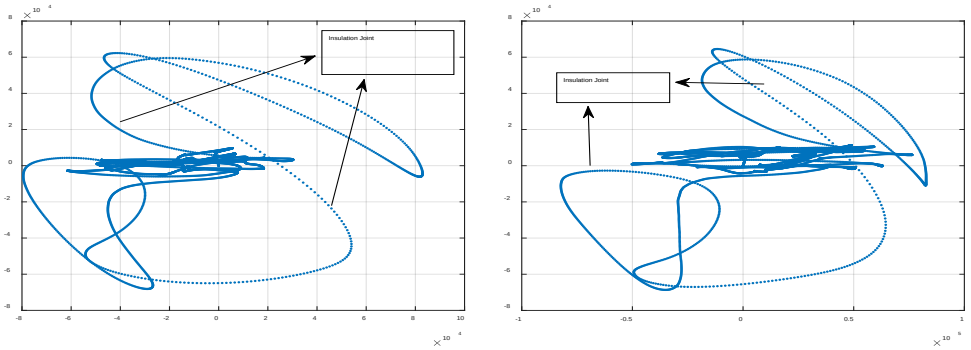

Figure 31I/Q plot of the demodulated signals: (a) 18 kHz Demodulation angle of 177 degrees and (b) 27 kHz Demodulation angle 327 degrees. Measurement of a section of lab test track to identify Rail Spike and Insulation Joint.

Figure 30 shows the time signal of the measurement carried out for a relatively healthy portion of the LTU test track with Rail Spike fasteners. Individual clamps can be easily distinguished from both 18 kHz and 27 kHz plots. The time signal also indicates the presence of Insulation joint present along the track. The demodulation angle was altered from that used for both the E-clip fasteners and Heyback. The IQ plot of the demodulated signal (Figure 31) shows that clamp features and insulation joints are modulated differently and can be distinguished from each other. The demodulation angle was fixed at 177degrees for 18 kHz and 327 degrees for 27 kHz.

8 Discussion

Figure12 through Figure.31 gives the time signal plot and the IQ plot associated with various measurements carried out using the Lindometer sensor. The time signal plots clearly shows that a very good correlation is achieved in the 1D signal between 18 KHz and 27 KHz signals, with a time delay. This correlation can be achieved for tracks with and without any defects and for any type of fastening system involved. Individual e-clips, Heyback clips and Rail spikes are easily distinguishable in the time signal. The demodulation angle remains the same for all signal processing for figures 12 through 27 and it is observed that the clamp angle for a particular fastener do not change depending on the condition of the track. However, the demodulation angle for different fastener varies as the geometrical shape of each fastener varies. Individual squats and cracks on the track are distinguishable both from the time signal and from the IQ-plot. It can be inferred from the IQ-plot (figure19, 23, 29 and figure 31) that the modulation angle for cracks, squats, e-clip, Heyback clip, rail spike, vibration and Insulation joints are all different from one another. Grinding marks on the track causes a small variation on the magnitude of the time signal. The effect of grinding marks is more seen in the IQ-plot of the demodulated signal, as it causes a slight roughness in the distribution. The sensor is capable of distinguishing between cracks and grinding marks as the angle of cracks remains different from other parameters. In addition, the grinding marks does not have any impact on the demodulation angle for the e-clip, the angle remains to be constant before and after grinding. There is a visible change in pattern to indicate the presence of missing fasteners both in the time signal and in the IQ-plot. However, further analysis is needed to identify the pattern difference for two or more missing e-clips in the same sleeper position.

The above tests were carried out for relatively short distances of the track. In order to carry out long distance measurements, modifications in the hardware of the sensor setup needs to be carried out.

9 Conclusion

The rail load is increasing at a very high rate and there is constant increase of railway use and loading capacity. Periodic monitoring of the railway track and its component plays a crucial role in maintenance strategy, to support both safety and profit making. The goal of this project was to develop an automatic train based detection system for rail and rail fastener inspection. Automated visual inspection are currently being employed for rail and fastener inspection, despite the fact that these modes of inspection requires huge investment. Further, these modes of inspection may not be reliable in adverse environmental conditions (submerged or obscured under debris/snow). An alternate approach that overcomes these challenges, by using differential eddy current based sensor, is recommended. This approach can provide faster scanning speed and faster feedback. The proposed inspection method is capable of simultaneously detecting faults on the track and the fasteners and distinguish between different kinds of fasteners. It can also efficiently distinguish between vibrations, cracks, squats, grinding marks and insulation joints along the track. Further investigations needs to be carried out to check the effectiveness of the Lindometer in detecting defects inside the rail.

Train based sensors are usually subjected to huge data volume. Hence, it becomes a priority to improve the MSU capability of the Lindometer to stream large amount of data. In addition, an upgrade in computational capability is also necessary to perform big data analytics. The detection algorithm for both the driving field also needs to be enhanced and improved, in order to quantify different crack types and to differentiate between different levels of grinding on the rail. More verifications that are extensive need to be carried out both in field and lab, where images or movies are synchronized to the measurement signals from the Lindometer, to observe the performance reliability of the sensor.

Improving the reliability and efficiency of the track and its components is a central problem in railway industry. This requires efficient condition monitoring techniques, including analytics for predicting and detecting faults, at the same time being able to manage huge data volumes. Machine learning for anomaly detection can be used as a strong tool to learn the anomalous behaviour from such huge data and make predictions based on the same. Anomaly detection based on supervised learning is not viable in the field, as it requires labelled training data that represents all relevant conditions pertaining to the track and its components. Labelled data for such huge variations requires huge investment for manual configurations and require skilled operators. Thus, investigation based on unsupervised methods of machine learning and anomaly detection that can function online without pre-training on labelled datasets must be considered.

The future scope of this project involves prototype development of the sensor to deal with big data, quantification of rail defects and developing efficient condition monitoring techniques with the aid of machine learning techniques to detect and predict faults from big data.

INFRA SWEDEN 2030

REFERENCES

1. Ambika Prasad Patr. Maintenance decision support models for railway infrastructure using rams and LCC analysis- PhD thesis
2. Ying Li, Hoang Trinh, Norman Haas, Charles Otto, Sharath Pankanti- Rail Component Detection, Optimization, and Assessment for Automatic Rail Track Inspection. IEEE transactions on intelligent transportation systems, vol. 15, no. 2, April 2014
3. Hao Feng, Z.Jiang, F.Xie, Ping Yang, Jun Shi, and Long Chen "Automatic Fastener Classification and Defect Detection in Vision-Based Railway Inspection Systems" IEEE transactions on instrumentation and measurement, vol. 63, NO. 4, APRIL 2014
4. J. Cunningham, A. Shaw, and M. Trosino. Automated track inspection vehicle and method, May 2000. US Patent 6,064,428.2
5. M. Trosino, J. Cunningham, and A. Shaw. Automated track inspection vehicle and method, Mar 2002. US Patent 6,356,299.
6. Francescomaria Marino and Ettore Stella- VISyR: a Vision System for Real-Time Infrastructure Inspection. Chapter from the book Vision Systems: Applications
7. P. De Ruvo, A. Distante, E. Stella, and F. Marino. A GPU based vision system for real time detection of fastening elements in railway inspection. In *Image Processing (ICIP), 2009 16th IEEE International Conference on*, pages 2333–2336. IEEE, 2009.
8. F. Marino, A. Distante, P. L. Mazzeo, and E. Stella. A realtime visual inspection system for railway maintenance: automatic hexagonal-headed bolts detection. Systems, Man, and Cybernetics, Part C: Applications and Reviews, IEEE Trans. On, 37(3):418–428, 2007
9. P. Babenko. Visual inspection of railroad tracks. PhD thesis, University of Central Florida, 2009.
10. A. Mahalanobis, B. V. K. V. Kumar, S. Song, S. R. F. Sims, and J. F. Epperson. Unconstrained correlation filters. Appl. Opt., 33(17):3751–3759, Jun 1994.
11. E. Resendiz, J. Hart, and N. Ahuja. Automated visual inspection of railroad tracks. Intelligent Transportation Systems, IEEE Trans. On, 14(2):751–760, Jun 2013
12. E. Stella, P. Mazzeo, M. Nitti, G. Cicirelli, A. Distante, and T. D'Orazio, "Visual recognition of missing fastening elements for railroad maintenance," in Proc. IEEE Int. Conf. Intell. Transp. Syst., Singapore, Sep. 2002, pp. 94–99
13. J. Yang, W. Tao, M. Liu, Y. Zhang, H. Zhang, and H. Zhao, "An efficient direction field-based method for the detection of fasteners on high-speed railways," Sensors, vol. 11, no. 8, pp. 7364–7381, Jul. 2011.
14. P. De Ruvo, A. Distante, E. Stella, and F. Marino, "A GPU-based vision system for real time detection of fastening elements in railway inspection," in Proc. 16th IEEE Int. Conf. Image Process., Cairo, Egypt, Nov. 2009, pp. 2333–2336.
15. G. De Ruvo, P. De Ruvo, F. Marino, G. Mastronardi, P. L. Mazzeo, and E. Stella, "A FPGA-based architecture for automatic hexagonal bolts detection in railway maintenance," in Proc. 7th Int. Workshop Comput. Archit. Mach. Percept., 2005, pp. 219–224.
16. Y. Xia, F. Xie, and Z. Jiang, "Broken railway fastener detection based on AdaBoost algorithm," in Proc. Int. Conf. Optoelectron. Image Process, vol. 1. Haiko, China, Nov. 2010, pp. 313–316.

17. Y. Li, C. Otto, N. Haas, Y. Fujiki, and S. Pankanti, “Component-based track inspection using machine-vision technology,” in Proc. 1st ACM Int. Conf. Multimedia Retr., Trento, Italy, 2011, no. 60
18. Y. Rubinsztejn, “Automatic detection of objects of interest from rail track images,” M.S. thesis, School Comput. Sci., Univ. Manchester, Manchester, U.K., 2011.
19. C. Mandriota, M. Nitti, N. Ancona, E. Stella, and A. Distante, “Filter based feature selection for rail defect detection,” Mach. Vis. Appl., vol. 15, no. 4, pp. 179–185, Oct. 2004.
20. M. Singh, S. Singh, J. Jaiswal, and J. Hempshall, “Autonomous rail track inspection using vision based system,” in Proc. IEEE Int. Conf. Comput. Intell. Homeland Security Personal Safety, Alexandria, VA, USA, Oct. 2006, pp. 56–59
21. P.L. Mazzeo, N. Ancona, E. Stella, and A. Distante, “Visual recognition of hexagonal headed bolts by comparing ICA to wavelets,” in Proc. IEEE Int. Symp. Intell. Control, Houston, TX, USA, Oct. 2003, pp. 636–641
22. D. Blei, A. Ng, and M. Jordan, “Latent dirichlet allocation,” J. Mach. Learn. Res., vol. 3, pp. 993–1022, Jan. 2003.
23. Hao Feng, Z.Jiang, F.Xie, Ping Yang, Jun Shi, and Long Chen “Automatic Fastener Classification and Defect Detection in Vision-Based Railway Inspection Systems” IEEE transactions on instrumentation and measurement, vol. 63, NO. 4, APRIL 2014
24. E. Jasiūniene and E. Ukauskas, “The Ultrasonic Wave Interaction with Porosity Defects in Welded Rail Head,” Ultrasound, Vol. 65, No. 1, 2010, pp. 12-18.
25. Sergio Martín del Campo Barraza Unsupervised Feature Learning Applied to Condition Monitoring-PhD thesis
26. Allan.M.Zarembski- “The Art and Science of Rail Grinding”- published by Simmons-Boardman Books -first edition, 2005
27. M Ph Papaelias, C Roberts, C LDavis “A review on non-destructive evaluation of rails: State-of-the-art and future development” *Proceedings of the Institution of Mechanical Engineers, Part F: Journal of Rail and Rapid Transit* Vol 222, Issue 4, pp. 367 – 384, October-21-2008
28. US Pat. 189,858. Mode of detecting defects in railroad rails, 1877.
29. Kube, K. Sperry trucks track troubles deep inside rails. Trains Mag., 2005, 20–21 February
30. Bray, D. E. Historical review of technology development in NDE. In Proceedings of the 15thWorld Conference on NDT, Roma, Italy, 2000
31. Clark, R. Rail flaw detection: overview and needs for future developments, NDT&E Int., 2004, 37, 111–118.
32. Thomas, H.-M., Heckel, T., and Hanspach, G. Advantage of a combined ultrasonic and eddy current examination for railway inspection trains. In Proceedings of ECNDT 2006, Berlin, Germany, 2006.
33. Krautkramer, J. and Kraukramer, H. Ultrasonic testing of materials, 4th ed., 1990 (Springer, Berlin, Germany).
34. 5 Bray, D. E. and Stanley, R. K. Non-destructive evaluation – a tool in design, manufacturing, and service, 1997, pp. 215–427 (CRC Press, West Palm Beach, FL).

35. Kenzo, M. Recent advancement of electromagnetic non-destructive inspection technology in Japan. IEEE Trans. Magn., 2002, 38(2), 321–326.
36. Drury, J. C. and Pearson, N. Corrosion detection in ferrite steels using magnetic flux leakage. In Proceedings of Magnetics in Non-Destructive Testing, London, UK, April 2005.
37. Pohl, R., Krull, R., and Meierhofer, R. A new eddy current instrument in a grinding train. In Proceedings of ECNDT 2006, Berlin, Germany, 2006.
38. Thomas, H.-M., Junger, M., Hintze, H., Krull, R., and Rühe, S. Pioneering inspection of railroad rails with eddy currents. In Proceedings of the 15th World Conference on Non-Destructive Testing, Rome, Italy, 2000.
39. Pohl, R., Erhard, A., Montag, H.-J., Thomas, H.-M., and Wüstenberg, H. NDT techniques for railroad wheel and gauge corner inspection. NDT&E Int., 2004, 37, 89–94.
40. Junger, M., Thomas, H.-M., Krull, R., and Rühe, S. The potential of eddy current technology regarding railroad inspection and its implementation. In Proceedings of the 16th World Conference on Non-Destructive Testing, Montreal, Canada, August–September 2004.
41. Mair, C. and Fararooy, S. Practice and potential of computer vision for railways. In IEE Seminar on Condition monitoring for Rail Transport, 10 November 1998.
42. Briggs, C. W. Developments in gamma ray radiography. Mater. Eval., 1976, 34(3), 14A–20A.
43. Rail track safety monitoring management system: rail inspect, EU funded project, Contract number: G3ST-CT- 2001-50169.
44. Forster, F. Theoretische und experimented Grundlagen der zerstorungfreien Werkstoffpriifung mit Wirbelstromverfahren. Zeitschrift fur Metallkunde, 43, pp. 163-171, 1952.
45. Mclntire, P. & McMaster, R.C. Nondestructive testing handbook, Vol. 4- The American Society for Nondestructive Testing, Columbus, Ohio, 1986.
46. Banks, J. & Hansford, D.C. Examination of surface cracks in carbon and manganese steel rails by the eddy current technique. British Journal ofNDT, 18, pp. 171-174, 1976.
47. T. Engelberg & F. Mesch, “Eddy current sensor system for non-contact speed and distance measurement of rail vehicles”. WIT Transactions on the Built Environment. Pp.10.2495/CR001231